Electrochemical, thermodynamic, and theoretical study of the corrosion inhibition properties of triglycidyloxy tripropylamine triazine on E24 steel in 1 M HCl

M.E. Ansar,[1]* K. Tassaoui,[1] A. Chraka,[2] R. Hsissou,[3] M. Damej,[1] H.T. Rahal,[4] S. El Hajjaji[5] and M. Benmessaoud[1]**

[1]Energy, Materials and Sustainable Development Team CERNE2D, Higher School of Technology Salé, Mohammed V University in Rabat, Morocco
[2]Laboratory of Engineering Materials and Sustainable Energy, Faculty of Science, Abdelmalek Essaadi University, Tetouan, Morocco
[3]Laboratory of Organic Chemistry, Bioorganic and Environment, Chemistry Department, Faculty of Sciences, Chouaib Doukkali University, El Jadida, Morocco
[4]Department of Chemistry, Faculty of Science, Lebanese International University, Lebanon
[5]Laboratory of Spectroscopy, Molecular Modelling Materials, Nanomaterial Water and Environment – CERNE2D, Faculty of Sciences, Mohammed V University in Rabat, Morocco
*E-mail: *med.elmahdi.ansar@gmail.com; **mohammed.benmessaoud@est.um5.ac.ma*

Abstract

The goal of this study is to investigate the corrosion inhibition characteristics of triglycidyloxy tripropylamine triazine (TGTPAT) on E24 steel in a 1 M hydrochloric acid medium. We used electrochemical methods (polarization curves and electrochemical impedance spectroscopy) to carry out this investigation. The polarization curves demonstrate that the TGTPAT mixed-type inhibitor has an inhibition effectiveness (IE%) of 92.11% at a dose of 10^{-3} M. The electrochemical impedance diagrams for all tested TGTPAT concentrations show that the inhibition occurs via a charge transfer mechanism on a heterogeneous surface; the IE% was 90.19 at 10^{-3} M, which was consistent with the results of dynamic polarization. The inhibitor adsorption on the metal surface was of the Langmuir type, with a negative ΔG_{ads} value indicating that the adsorbed layer on the metal surface is stable. Furthermore, the ΔG_{ads} approach value of 40 kJ/mol relates to charge transfer between TGTPAT inhibitor molecules and the metal surface E24 (chemisorption), resulting in the formation of covalent or coordination bonds. SEM/EDX analysis: after 20 hours of immersion in the corrosive solution with an inhibitor, it was confirmed that the surface of the metal was protected and homogeneous. Peaks of iron, oxygen, and carbon are also visible, indicating the presence of the inhibitor's components on the surface. An investigation into the effect of increasing temperature revealed that as temperature rises, so does the corrosion current density, resulting in a decrease in inhibitor efficiency. Quantum chemical calculations of TGTPAT corrosion inhibitors were performed to investigate the effect of molecular structure on inhibition efficiency.

Received: April 24, 2024. Published: December 30, 2024 doi: 10.17675/2305-6894-2024-13-4-38

Keywords: *corrosion, polarization, impedance spectroscopy, TGTPAT, DFT.*

1. Introduction

Polyepoxide resins are currently commonly utilized as corrosion inhibitors to prevent E24 steel from corroding in hydrochloric acid [1–3]. The polyepoxide resins (TGTPAT) contain aromatic rings and heteroatoms (S, N, and O). They are commonly referred to as corrosion inhibitors [4–6]. These can transfer electrons to the metal's surface, occupying unoccupied orbitals and forming covalent connections. The efficiency of heteroatoms in adsorption processes changes in the following manner: S > N > O. Carbon steel is more extensively employed in the industry because of its inexpensive cost [7].

In industry, hydrochloric acid is frequently used for stripping and cleaning [8]. Because of this acidic solution's aggression, corrosion inhibitors are used to slow down the pace at which metals corrode [8]. The primary causes of polymer inhibitor adsorption include the interactions between the inhibitors' macromolecular structure and the metal surface, as well as the physicochemical characteristics of the polymer associated with its functional group [9, 10]. This suggests that the protective film is forming more firmly [11]. The application of density functional theory (DFT) to inhibitors for polyepoxide resins confirms the inhibition mechanism, that works with this type of inhibitor [12].

This research aims to assess the performance of triglycidyloxy tripropylamine triazine (TGTPAT) on E24 steel in 1 M hydrochloric acid medium. Epoxy resin was made in our laboratory as a corrosion inhibitor for E24 steel in 1 M hydrochloric acid [12]. The interaction between the inhibitory matrix and metallic surface is studied using several approaches, including gravimetric and electrochemical (stationary and transient) [12]. Finally, molecular dynamics simulations support the experimental findings.

2. Material and Methods

2.1. Preparation of metal and corrosive medium

Table 1 lists the chemical composition of the metal used in this investigation, E24. The specimens were chosen to have a 10 mm^2 circular surface area. Before each test, the specimen was polished with grade 600, 1200, and 1500 sandpapers, cleaned with distilled water and alcohol, and then air dried.

Table 1. Chemical composition of the metal used E24.

C%	Si%	P%	S%	Ti%	Co %	Cr%	Mn%	Fe%
0.11	0.24	0.021	0.16	0.011	0.009	0.077	0.47	99.046

The corrosive medium is a 1 M HCl solution produced from distilled water and a commercial hydrochloric acid solution (37%). The TGTPAT inhibitor doses used varied from $5 \cdot 10^{-2}$ to 10^{-3} M.

2.2. Synthesis of triglycidyloxy tripropylamine triazine

The novel trifunctional polyepoxide resin, namely triglycidyloxy tripropylamine triazine (TGTPAT), was synthetized using condensation reaction according to procedures reported in several publications [13, 14]. In the first step, we condensed $4.864 \cdot 10^{-3}$ mol of propanol amine (purity of 97%) with $3.201 \cdot 10^{-3}$ mol of 2,4,6-trichloro-1,3,5-triazine (purity of 98%) by using ethanol as solvent under magnetic stirring at 80°C for 24 hours. In the second step, we added $5.854 \cdot 10^{-3}$ mol of epichlorohydrin (purity of 99%) to the reaction mixture under magnetic stirring at 65°C for 4 hours. In addition, we added $7.867 \cdot 10^{-3}$ mol of triethylamine (purity of 99,5%) under magnetic stirring at 40°C for 3 hours (Scheme 1). Besides, the excess of ethanol was eliminated by using the rotary evaporator.

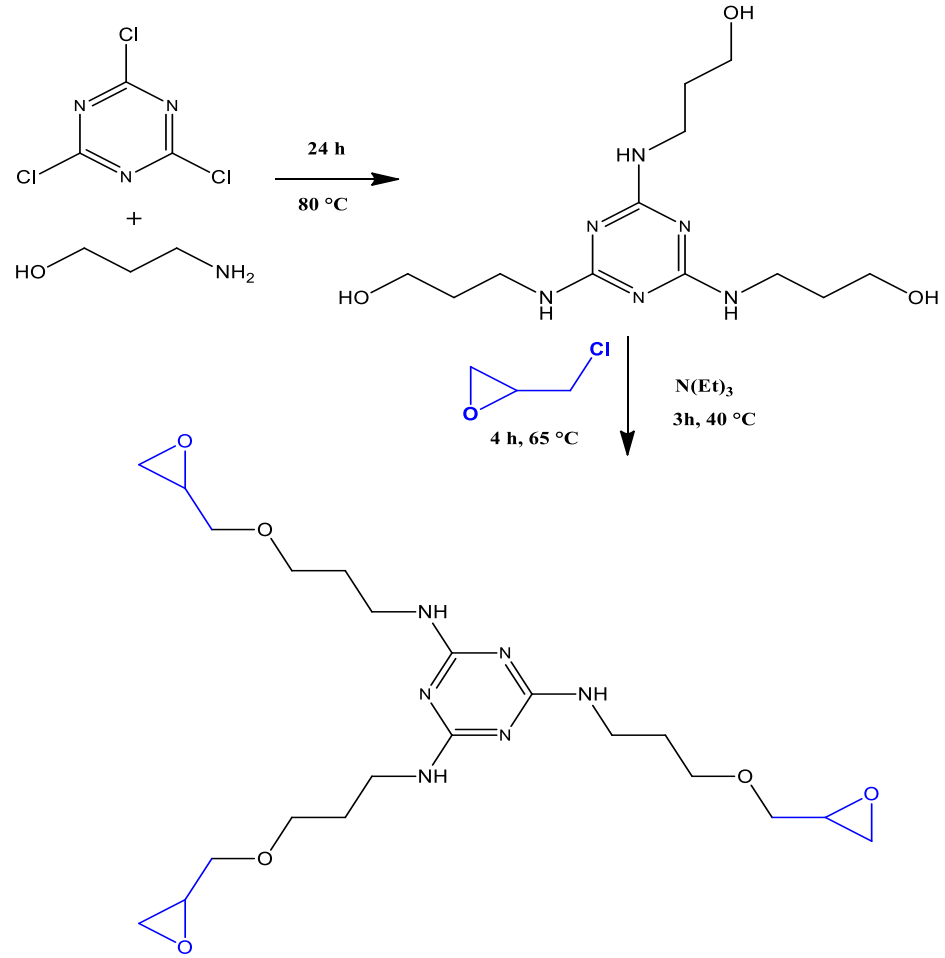

Scheme 1. Synthesis of TGTPAT.

2.3. Electrochemical measurements

The electrochemical examination was carried out with the help of a Volta Master software-driven potentiostat PGZ 100. For the studies, a three-electrode cell with a carbon steel (E24) working electrode, a saturated calomel reference electrode, and a platinum (Pt) electrode functioning as a counter was utilized. The working electrode was immersed in a corrosive

solution for 60 minutes in a quasi-stationary state at an open circuit potential prior to any electrochemical analysis. Polarization curves between −800 and −100 mV were produced using a scanning rate of 1 mV/sec around an open-circuit potential. Electrochemical impedance spectroscopy graphs were acquired from $10 \cdot 10^4$ Hz to $10 \cdot 10^{-3}$ Hz. The inhibitory effectiveness (IE%) for polarization curves was calculated using the equation [15]:

$$IE\% = \frac{i^0 - i^{in}}{i^0} \times 100 \quad (1)$$

where i^0 is the corrosion current densities uninhibited and i^{in} is corrosion current densities inhibited with various concentrations of TGTPAT. The equation below [16] was used to calculate the inhibition efficiency *IE*% from electrochemical impedance spectroscopy (EIS) plots.

$$IE\% = \frac{R_p^{in} - R_p^0}{R_p^{in}} \times 100 \quad (2)$$

where R_p^{in} and R_p^0 indicate the polarization resistance inhibited, and polarization resistance uninhibited with diverse concentrations of TGTPAT, respectively.

2.4. Scanning electron microscopy/Energy Dispersive X-ray Analysis

SEM (scanning electron microscopy) allows for the selection of surfaces to be analyzed based on many microstructural parameters. The micrograph of the E24 surface was investigated after 20 hours of immersion in the acid media without and with TGTPAT, and the chemical composition was characterized by an analysis of Energy Dispersive X-ray [17].

2.5. Computational details

2.5.1. DFT modeling

Density Functional Theory (DFT) method was used in this work to predict the structural and global reactivity of the neutral form of TGTPAT (Figure 1). The optimizing the geometrical structure of the title molecule was done by Becks three-parameter exchange functional B3 with Lee–Yang–Parr (B3LYP) level at 6-311++G(d,p) basis set in a gas phase [19, 20]. DFT calculations were performed using Gaussian 09 program package [21]. The DFT calculations was carried out in an aqueous phase by the self-consistent-field (SCRF) theory based on the integral equation formalism variant (IEF-PCM) method [22]. The validity of employing the IEF-PCM method to study the solvent effect in research related to corrosion inhibitors has been demonstrated in the literature [23, 24]. The DFT study has been used for analyzes of Frontier Molecular Orbitals (FMOs), Molecular Electrostatic Potential (MEP), Mulliken charge distribution, and electronic descriptors including the energies of highest occupied, lowest unoccupied molecular orbital (E_{HOMO} and E_{LUMO}), the frontier orbital energy gap (E_{gap}), the electron affinity (*A*), the ionization potential (*I*), the dipole moment (μ), the electronegativity (χ), the chemical potential (η), the chemical hardness (η), the softness (*S*),

the electrophilicity index (ω), the nucleophilicity index (ε), the fraction of transferred electrons (Δ*N*) and metal/inhibitor interaction energy (Δψ) were calculated according to Eqs. (3–12) as reported in the literature [25, 26]:

$$A = -E_{\mathrm{LUMO}} \tag{3}$$

$$I = -E_{\mathrm{HOMO}} \tag{4}$$

$$\Delta E_{\mathrm{gap}} = E_{\mathrm{LUMO}} - E_{\mathrm{HOMO}} \tag{5}$$

$$\chi = \frac{(I + A)}{2} \tag{6}$$

$$\eta = \frac{(I - A)}{2} \tag{7}$$

$$S = \frac{1}{\eta} \tag{8}$$

$$\omega = \frac{\chi^2}{2\Psi} \tag{9}$$

$$\varepsilon = \frac{1}{\omega} \tag{10}$$

$$\Delta N = \frac{\chi - \chi_{\mathrm{inhibitor}}}{2(\chi + \chi_{\mathrm{inhibitor}})} \tag{11}$$

$$\Delta\Psi = \frac{(\chi - \chi_{\mathrm{inhibitor}})^2}{4(\eta - \eta_{\mathrm{inhibitor}})} \tag{12}$$

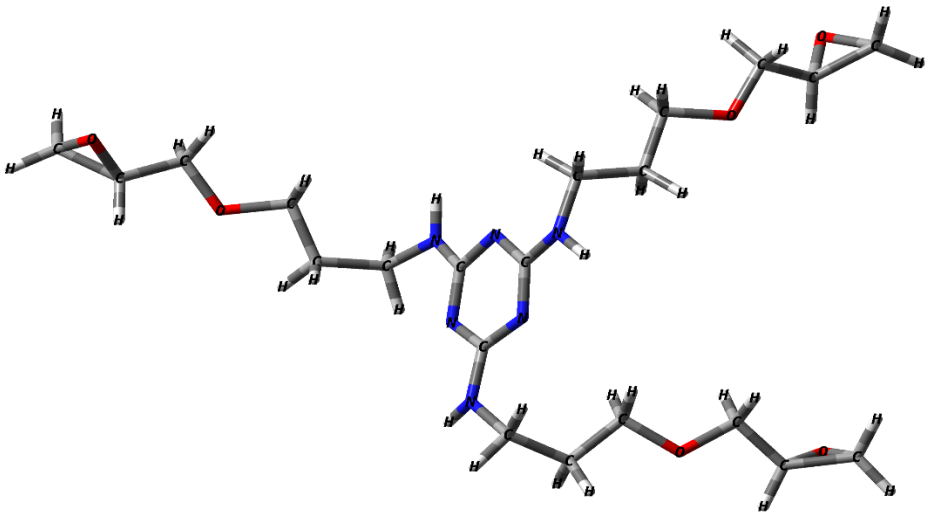

Figure 1. Chemical structure of TGTPAT.

2.5.2. Molecular dynamics (MD) and Monte Carlo (MC) simulations approach

To study the nature of the interaction between the TGTPAT and Fe-substrate, we used the Metropolis Monte Carlo (MC) and molecular dynamics (MD) methodology [27, 28] implemented using the Material Studio 8.0 software from the BIOVIA company [11]. For running MC/MD simulations of the interaction between the TGTPAT molecule of neutral form and E24-surface were carried out with a E24 supercell of size (14×14) and a vacuum slab with (6.0 nm) thickness in a simulation box (3.4 nm × 3.4 nm × 6.8 nm) with periodic boundary conditions to simulate the current effective part of the Fe-substrate, without any arbitrary boundary effects [29]. The aqueous phase has been examined in this simulation using water molecules ($500H_2O$), along with corrosive species, namely corrosive hydroniums ($6H_3O^+$) and chloride ions ($6Cl^-$), as well as the title compound, with each metal surface to approximate the real condition. The MC/MD calculations were performed using the COMPASS Force Field [30] to optimize the structures of all system components (metal surface/inhibitor/corrosive species). The "Ewald" and "atom-based" summation methods were applied for the "Electrostatic" and "van der Waals" non-bonding interactions respectively [31]. Furthermore, MC calculations were performed using five cycles (15000 steps each cycle) of simulated annealing at 293 K. Furthermore, MD was achieved using an NVT canonical ensemble at 293 K, 1 fs time step, and 400 picoseconds simulation period. This study was used to find low-energy adsorption sites to study the optimal adsorption of a single inhibitor molecule on the E24 surface, aiming to discover the relationship between the effect of its molecular structure and its inhibition efficiency.

3. Results and Discussion

3.1. FTIR analysis

Triglycidyloxy tripropylamine triazine (TGTPAT) polyepoxide resin synthesized was identified through using the Fourier transform infrared (FTIR) to determine and identified the varying functional groups. Furthermore, the different bands of FTIR are displayed follows: 3341 cm^{-1} was corresponding to the stretching vibrations of the amine function (−NH). Besides, the absorption band situated at 2930 cm^{-1} was attributed to the stretching vibration of aliphatic methylene group. Furthermore, the absorption band located at 1467 cm^{-1} was corresponding to the C=N of heterocyclic compound. Also, the absorption band appeared at 1084 cm^{-1} can be attributed to the unsymmetrical stretching vibration of the C−O−C ether function. In addition, the presence of the epoxide oxiran was indicated by the characteristic absorption band at 830 cm^{-1}.

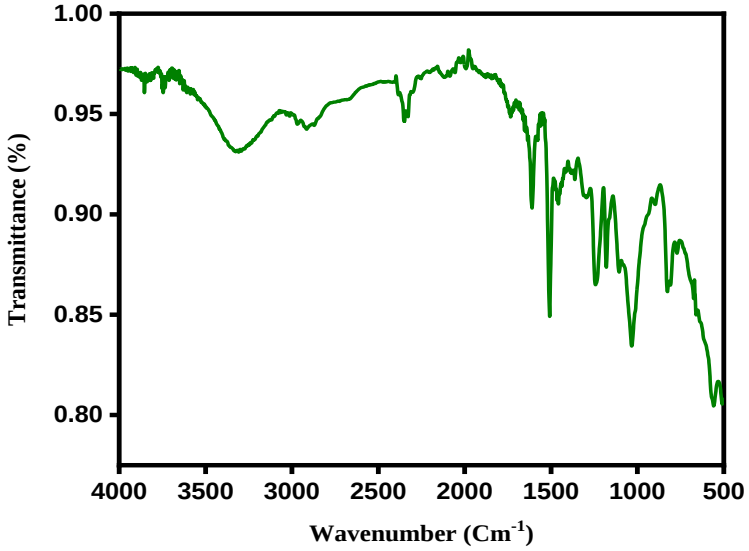

Figure 2. FTIR of TGTPAT.

3.2. Electrochemical measurements

3.2.1. Evolution of the free potential as a function of time

Monitoring the free potential as a function of time, or open circuit potential, will assist in comprehending the behavior of a material in contact with a humid, corrosive environment [18]. It provides information on the preliminary changes as well as the nature of the activities that are taking place at the metal/electrolyte interface.

Initially, the OCP versus time curves become parallel to time (Figure 3), indicating that the oxide layer accumulated on the surface of the metal E24 has been removed and that, in the inhibited cases, the adsorption of the TGTPAT inhibitor molecules has been obtained in an immersion time of nearly 0.33 h. On careful examination, it can be seen that, compared to the uninhibited case, in the inhibited cases, the OCP curves versus time at some selected concentrations (0.05 mM and 0.1 mM) shifted towards positive values (anodic), while at other concentrations (0.5 mM and 1 mM), the curves moved towards negative values (cathodic).The shift of the OCP curves versus time in the positive direction indicates that TGTPAT at these selected concentrations act as an anodic type of this inhibitor and that it adsorbs to the anodic sites of the carbon steel, retarding or slowing its anodic dissolution. While the negative shift of the OCP curves versus time indicates that the TGTPAT inhibitor at these chosen concentrations behaved as a cathodic type, then the TGTPAT molecules adsorb to the cathodic sites and make the release process difficult for hydrogen. These observations suggest that TGTPAT acts as a mixed-type inhibitor [19].

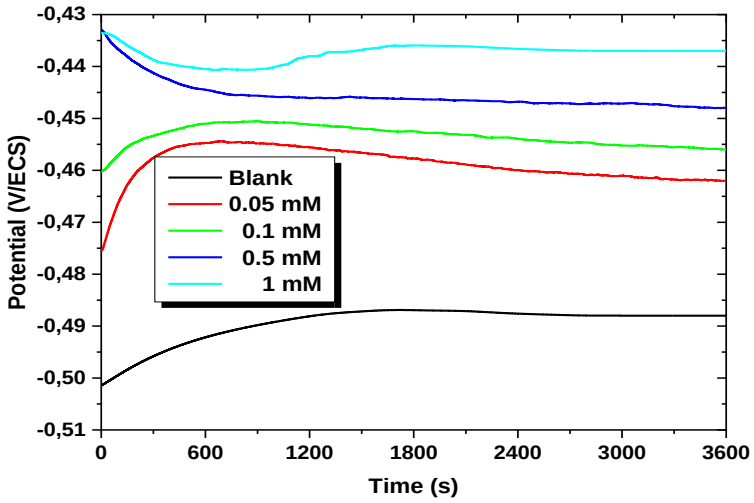

Figure 3. Evolution of the free potential as a function of immersion time for E24 steel in 1 M HCl solution at different concentrations of TGTPAT at 293K.

3.2.2. Potentiodynamic polarization measurements

Figure 3 depicts the polarization curves, and Table 2 reports the parameters corresponding to the extrapolation of the parameters of E_{corr}, i_{corr}, βa, and βc, as well as the inhibitory efficiency *EI*(%) and the rate of carbon steel surface coverage [20].

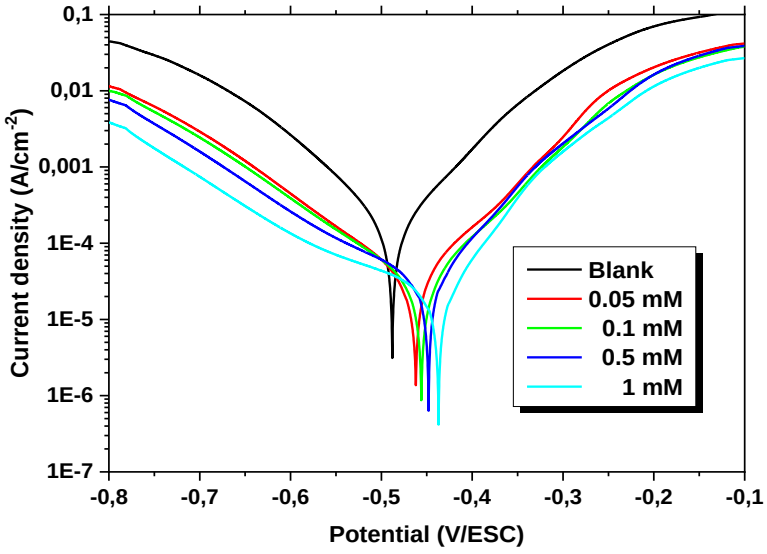

Figure 4. Potentiodynamic polarization curves of E24 steel in 1 M HCl in the absence and in the presence of different concentrations of TGTPAT at 293K.

Figure 4 confirms that the presence of TGTPAT decreases in the anodic and cathodic current densities; this can be attributed to the adsorption of the TGTPAT inhibitor molecules on the active sites of the E24 surface, which retards both the anodic dissolution of the metal and the cathodic discharge of hydrogen, hence the corrosion process is slowing down.

Table 2 clearly shows that when TGTPAT concentration increases, i_{corr} values fall dramatically. The i_{corr} is sufficient for the 1 M (216.8 mA/cm^2) HCl solution, but it is reduced (17.11 mA/cm^2) with 1 mM of TGTPAT. The slope values of Tafel (βa) anodic lines change with the addition of TGTPAT, indicating that the inhibitor studied was initially adsorbed on the metal surface and obstructed by simply blocking the reaction sites of the metallic surface without affecting the anodical reaction mechanism [35]. Furthermore, the (βc) values for TGTPAT vary with the addition of TGTTAT, indicating that the mechanism of the hydrogen release process is altered in the presence of TGTRAT. The table also shows that inhibitory efficacy increases with concentration, and the highest inhibition (92.11%) was observed at 1 mM.

Table 2. Electrochemical parameters of E24 steel at various concentrations of TGTPAT in 1 M HCl and corresponding inhibition efficiency IE%.

[TGTPAT] (mM)	E_{corr} (mV/Ag-AgCl)	i_{corr} (μA/cm^2)	βc (mV/dec)	βa (mV/dec)	*EI*(%)
0	–488	216.8	–93.3	86.9	
0.05	–462	40.74	–133	103.4	81.21
0.1	–456	28.23	–129.6	90.3	86.98
0.5	–448	23.18	–159.2	73.6	89.31
1	–437	17.11	–209.4	65.5	92.11

3.2.3. Electrochemical impedance spectroscopy

We plotted electrochemical impedance diagrams obtained at different concentrations of the inhibitor TGTPAT in a frequency range between 10^4 Hz and $10 \cdot 10^{-3}$ Hz to better understand the corrosion and protection mechanisms that occur on the surface of the steel, which are shown in the Nyquist diagram in Figure 5. Table 3 shows the values of the corresponding electrochemical parameters and the inhibitory efficiency *EI*(%), as well as the error adjustment factor.

Initially, we observe that for all inhibitor concentrations ranging from 10^{-3} M to 10^{-5} M, the impedance spectrum consists of a single capacitive loop well centered on the real axis, suggesting that the corrosion process has not changed and continues to proceed through charge transfer.

According to the parameters in Table 3 and the impedance diagram (Figure 5), we can conclude that, first; the addition of the inhibitor increases the size of the impedance spectrum, which has the shape of a semi-circle that is more or less flattened, indicating the formation

of a protective layer. Second, the inhibitory effectiveness of the inhibitor, TGTPAT, rises with its concentration, peaking at 92.11% at 10^{-3} M. This demonstrates that this chemical has an effective inhibitory impact on the corrosion of E24 steel in 1 M hydrochloric acid [36].

On the other hand, the decrease in C_{dl} is caused by the adsorption of the organic inhibitor on the surface of E24 steel, which reduces the active surface of the electrode, resulting in corrosion protection provided by molecules absorbed on the electrode surface through interactions between the electron pairs of the heteroatoms and the steel surface [37]. The flattened shape of the capacitive loops is due to the change in frequency dispersion caused by the heterogeneity of the electrode surface [21, 38–40], thus we used the equivalent electrical circuit depicted in Figure 6 to solve this. This circuit consists of the electrolyte resistance (R_s), a constant phase element (CPE) that replaces the double layer capacitance (C_{dl}) to account for the previously mentioned inhomogeneity, and a charge transfer resistance (R_{ct}).

Table 3. Electrochemical Impedance parameters for corrosion of E24 steel in 1 M HCl without and with the different concentrations of TGTPAT.

[TGTPAT] (mM)	R_s **(Ω·cm²)**	R_{ct} **(Ω·cm²)**	C_{dl} **(μF·cm⁻²)**	***n***	***EI*(%)**	θ
0	1.937	38.77	473.59	0.96245		
0.05	1.825	224.6	111.96	0.85827	82.74	0.8274
0,1	1.721	252.6	99.55	0.84572	84.65	0.8465
0.5	1.622	334.3	75.22	0.83446	88.40	0.8840
1	1.721	395.3	63.61	0.79895	90.19	0.9019

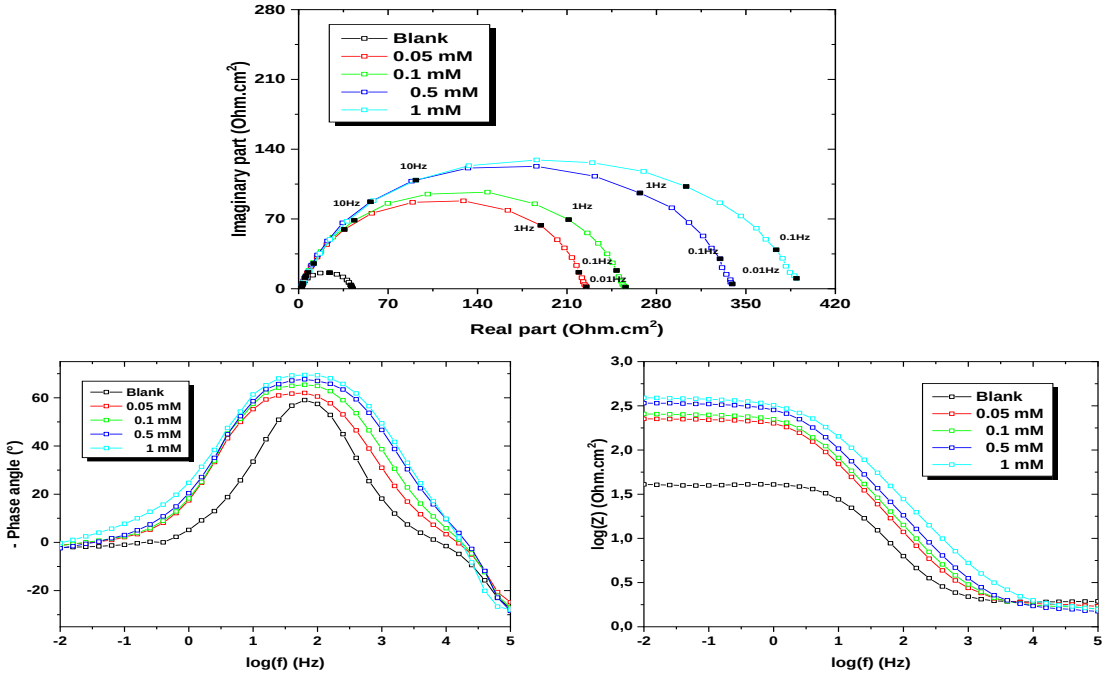

Figure 5. Nyquist, Bode, and phase angle diagrams for E24 steel in 1 M HCl without and with the different concentrations of TGTPAT at 293 K.

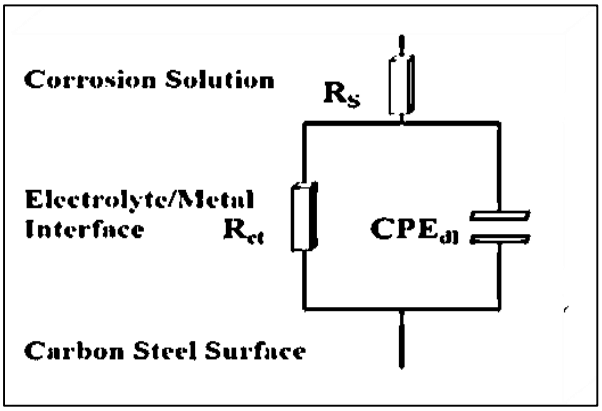

Figure 6. Equivalent circuit for E24 in 1 M HCl interface with and without the different concentrations of TGTPAT at 293 K.

3.3. Adsorption isotherm

Basic information on the interaction between the inhibitors and the mild steel surface and the mechanism of electrochemical reaction may be provided by the adsorption isotherm [21].

Our inhibitor (TGTPAT) used in this study obeys the Langmuir isotherm. According to the Langmuir isotherm, Θ is linked to the inhibitor concentration C_{inh} by the following equation [22]:

$$\frac{C_{\text{inh}}}{\theta} = \frac{1}{K_{\text{ads}}} + C_{\text{inh}} \tag{13}$$

$$K_{\text{ads}} = \frac{1}{55.5} e^{-\left(\frac{\Delta G^0_{\text{ads}}}{RT}\right)}$$

where C_{inh}, K_{ads}, and ΔG^0_{ads} are the concentration of TGETPT, the equilibrium constant of the adsorption process and free energy of adsorption, respectively.

The values of the correlation coefficient (R^2) are close to Langmuir adsorption isotherm one (Figure 7). This indicates that the adsorption of the TGTPAT inhibitor on the surface of E24 steel in 1 M HCl medium obeyed the Langmuir adsorption isotherm.

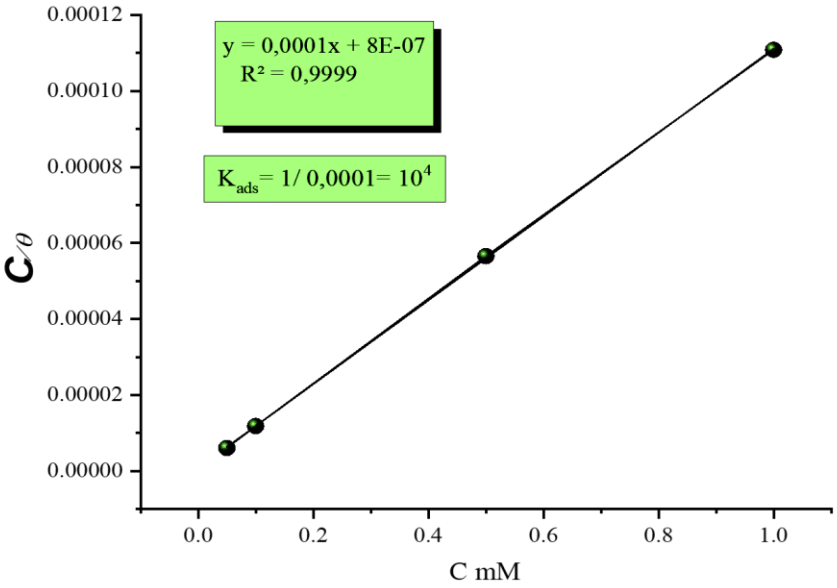

Figure 7. Langmuir adsorption isotherms for E24 in 1 M HCl in the presence of TGTPAT.

Table 4. Parameters of adsorption of the TGTPAT inhibitor.

Inhibitor	K_{ads} **(mol^{-1}·L)**	R^2	ΔG^0_{ads} **(kJ·mol^{-1})**
TGTPAT	10^4	0.9999	–32.22

The calculated value of ΔG^0_{ads} in table 4 is negative, signifying that the adsorbed layer on the metal surface is stable. Moreover, the value of ΔG^0_{ads} is close to –40 kJ/mol, which shows that the charge transfer between the TGTPAT inhibitor molecules and the E24 metal surface is chemisorption with the formation of covalent or coordination bonds [23], [24], [25].

3.4. Temperature effect

Temperature influences the stability of an inhibitor in an aggressive environment. Temperature increases can enhance inhibitor desorption and lead to the fast breakdown of the organic compounds or complexes produced, decreasing the steel's corrosion resistance [26].

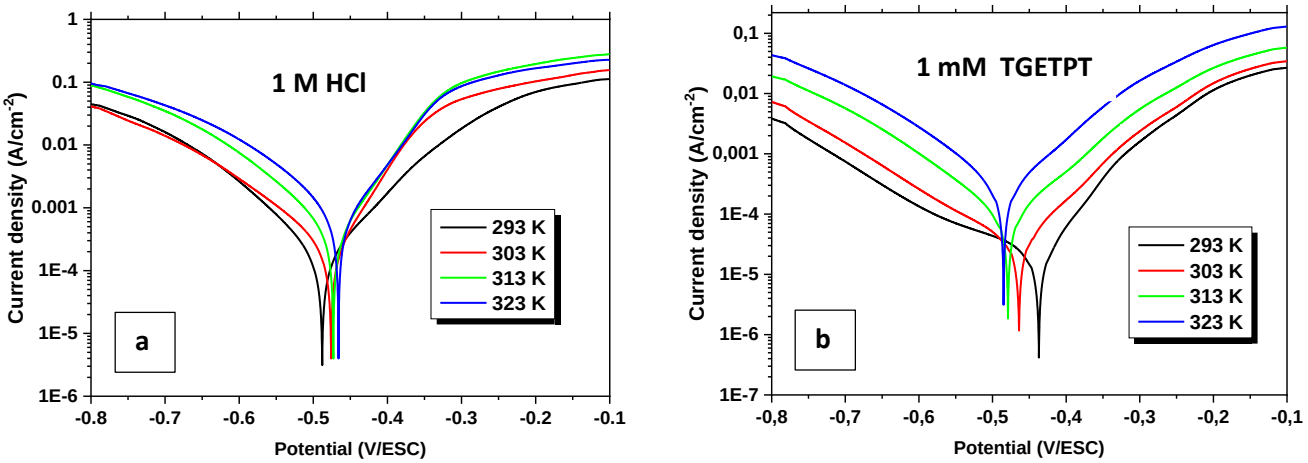

Figure 8. Polarization curves of E24 steel in 1 M HCl solution obtained (a) in the Blank and (b) at 10^{-3} M of TGETPT.

Table 5. Corrosion current density and inhibitory efficiency at different temperatures for 10^{-3} M of TGETPT.

[TGTAT] (M)	***T* (°K)**	**E_{corr} (mV/Ag-AgCl)**	**i_{corr} (μA/cm²)**	**β_c (mV/dec)**	**β_c (mV/dec)**	***EI*(%)**
0 M	293	–61.65	216.8	–93.3	86.9	
	303	–476	234.7	–112.6	60.4	
	313	–473	341.7	–85.1	62.1	
	323	–466	735.6	–100.8	74.6	
10^{-3} M	293	–437	17.11	–209.4	65.5	92.11
	303	–464	33.68	–157.1	92.5	85.65
	313	–479	90.21	–110	106.9	73.60
	323	–485	223.6	–108.1	97.6	69.60

Table 5 and Figures 8(a) and 8(b) present the findings of the temperature effects analysis. These findings indicate that an increase in temperature leads to an increase in corrosion speed and, consequently, a decrease in inhibitory efficiency *EI*(%) for each concentration under study. This is especially noticeable for temperatures of 313K and 323K.

This is because the temperature factor affects how E24 steel behaves in the acidic HCl medium, which in turn affects the metal-inhibitor interaction [46]. As a result, the temperature increases, speeding up the steel's dissolution process and causing a partial desorption of TGTPAT molecules on the surface of the E24 steel. These findings also suggest that the TGTPAT compound has a good effect on corrosion resistance in the temperature investigated (293 to 323 K).

3.5. Surface analysis

3.5.1. Scanning electron microscope

Validation of the adsorption of the inhibitor on the surface of E24 was carried out by employing scanning electron microscopy (SEM). In this research, scanning electron microscopy (SEM) was used to observe the topography of the sample in secondary electron imaging.

After immersion for 24 hours in HCl solution, the sample was subjected to analyses with and without the addition of 1 mM TGTPAT. Figure 9 reveals the results of these analyses.

The HCl solution caused severe corrosion of the surface of the working electrode (Figure 9.A), leading to the creation of a porous film of oxides, notably Fe_2O_3 and FeO. However, the addition of the inhibitor TGTPAT (Figure 9.B) resulted in the creation of a protective layer. This adsorption suppressed the corrosion process and modified its behavior.

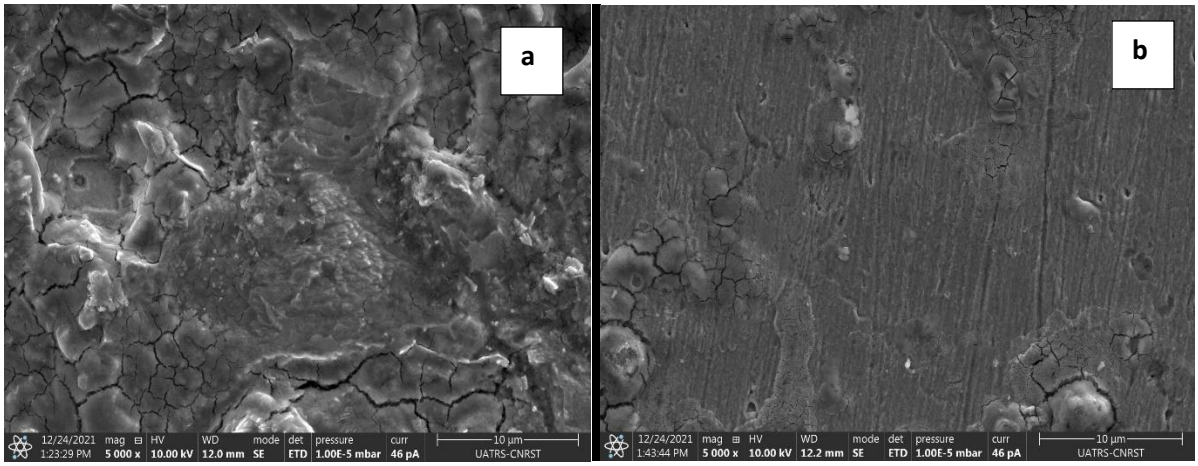

Figure 9. SEM image of E24 surface after immersion for 24 h in 1 M HCl without (a) and with 10^{-3} M of TGETPT (b).

3.5.2.EDX analysis

The analysis carried out using EDX spectrometry (Figure 10A) revealed the presence of characteristic photos corresponding to the constituent elements of iron and oxygen. In the presence of MTS (Figure 10B), the EDX spectra showed additional photos associated with the formation of a protective film of inhibitors on the surface of the working electrode. From then on, the iron and oxygen photos showed reduced intensity compared to the uninhibited

sample. This observation indicates the creation of a protective layer on the surface of the E24 alloy.

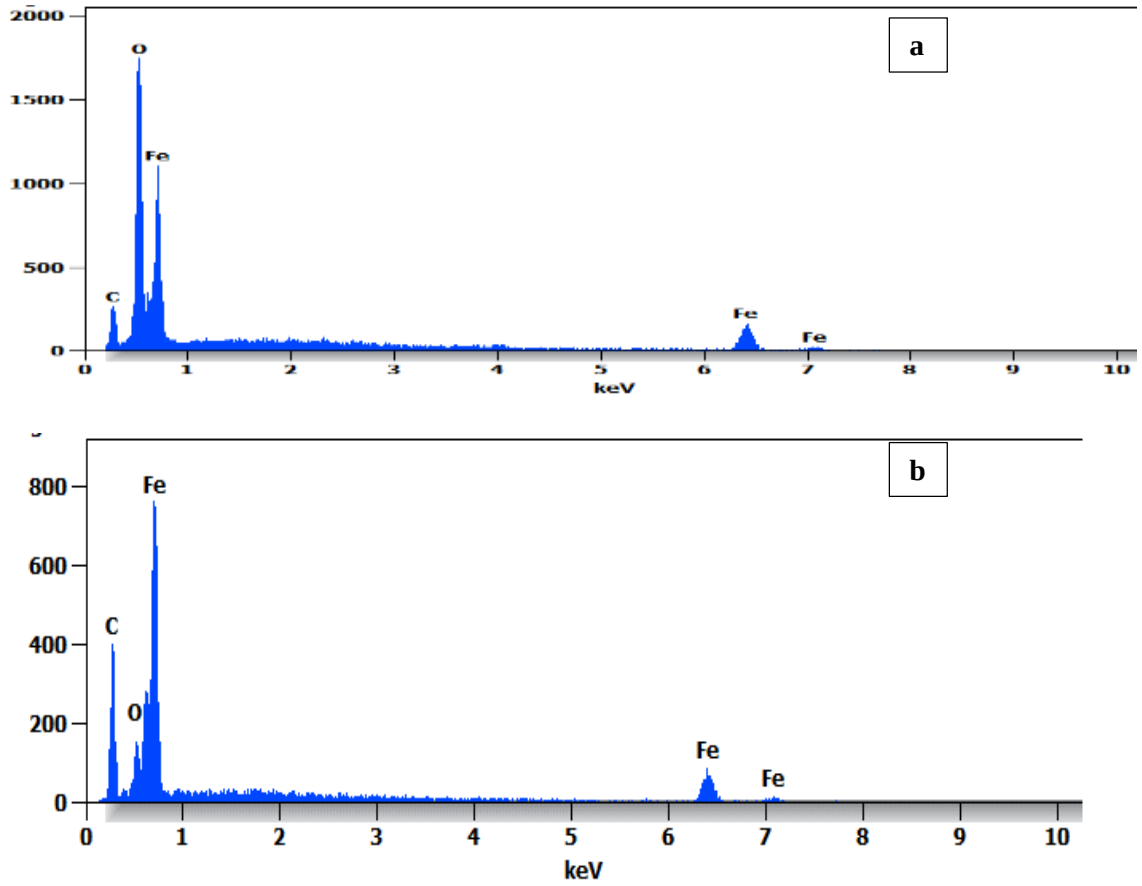

Figure 10. EDX of the surface condition of mild steel submerged in 1 M HCl for 24 hours: (a) in the absence of inhibitor, (b) in the presence of 10^{-3} M in TGTPAT.

3.6. DFT Calculations

The DFT method has shown to be quite useful in identifying molecule structures, electronic properties, and molecular reactivity. The usefulness of this strategy has been boosted by amazing advances in supercomputing capabilities [47, 48]. Experimenting with corrosion inhibition and discovering its causes can take time and resources. Therefore, DFT-based theoretical simulations were used to analyze the interactions between the inhibitor molecules and the metal surface, thereby providing essential insights into the inhibition processes [49, 50].

3.6.1. Optimized structure

We ran a conformational analysis on compound TGTPAT to find the most stable conformations. The most stable conformations were then extensively tuned. Figure 11 illustrates the optimized molecular structure of TGTPAT, with labels and atoms numbering.

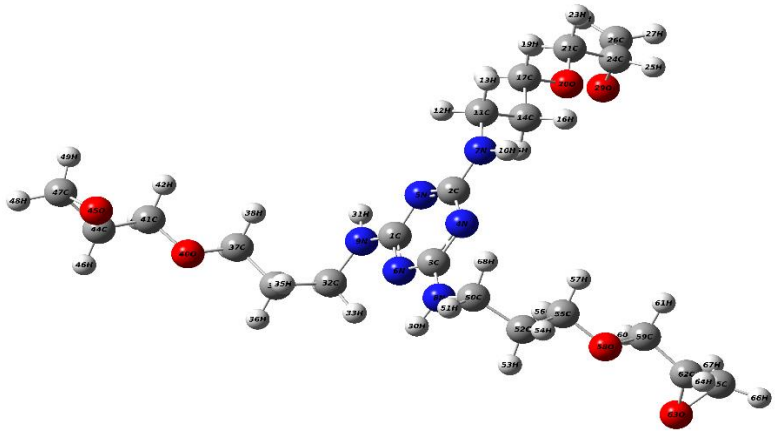

Figure 11. Optimized structures of TGTPAT computed calculated by DFT method at B3LYP/6-311++G(d,p) levels of theory.

3.6.2. Frontier molecular orbitals (FMOs)

In this study, we used the Ab-initio calculations based on DFT at by means of B3LYP/6-311++G(d,p) level of theory to understand the results of the high inhibition efficiency of TGTPAT (*E* = 92.11%), as well as to evaluate the relationship between this inhibition efficiency and molecular structure. The study of frontier molecular orbitals (FMOs) plays an important part in understanding chemical reactions and electronic properties. The highest occupied molecular orbitals (HOMO) are able to serve as an electron-donating and the lowest unoccupied molecular orbitals (LUMO) are able to serve as an electron-accepting [50, 51]. The FMOs surfaces of TGTPAT in the neutral forms are shown in Figure 12. The orbital distributions HOMO and LUMO are distributed almost over the entire surface of TGTPAT. The negative and positive areas are indicated by the red and green colors, respectively. As shown in Figure 12, both HOMO and LUMO distributions are firmly located over the lone pairs of electrons on the nitrogen (N) and oxygen (O) atoms and C=C bonds. This observation suggests that areas of this compound develop the strongest tendency to accept and donate electrons, which also makes them a great corrosion inhibitor [52, 53].

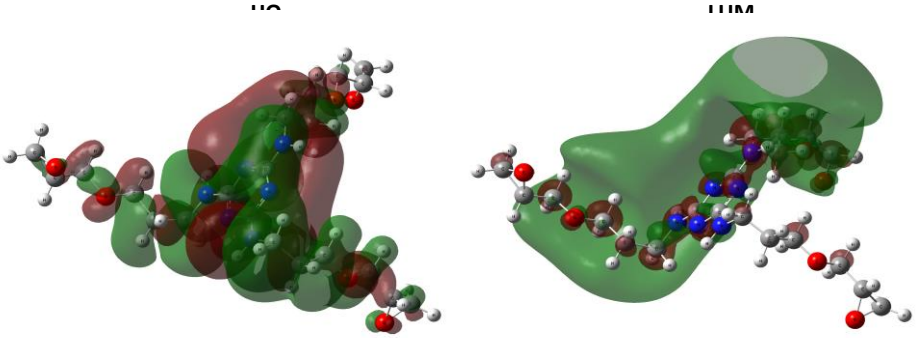

Figure 12. The HOMO-LUMO of neutral form of TGTPAT computed at DFT- B3LYP/6-311++G(d,p) level of theory.

3.6.3. Global reactivity descriptors

For more information on the inhibitory capacity of the title compound, we used some quantum chemical indices of TGTPAT by means of B3LYP/6-311++G(d,p) level of theory. The calculated are listed in Table 6. As reported in the literature [23, 24], the analysis of the frontier molecular orbitals (E_{HOMO} and E_{LUMO}) it gives important predictions about the interactions of corrosion inhibitors onto the metal surface involve donor-acceptor ability and during these interactions, E_{HOMO} is related to the electron-donating ability of the inhibitor compound and E_{LUMO} is related to the electron-accepting ability of the inhibitor compounds from the fulfilled metal orbital (d). Therefore, the highest occupied molecular orbital energy (E_{HOMO}) and the lowest unoccupied molecular orbital energy (E_{LUMO}) are associated with strong metal-inhibitor bindings and thereby high protective ability [54].From Table 6, the results showed that the values of E_{HOMO} and E_{LUMO} of the TGTPAT by using the B3LYP/6-311++G(d,p) level of theory are –6.331 eV and –0.405 eV, respectively. which indicates that our title molecule is an electron donor-acceptor [25]. On the other hand, a lower (ΔE_{gap}) is related to high chemical reactivity and adsorption ability of the molecule [55]. It is clear from the results presented Table 1 that the values of ΔE_{gap} were estimated at about 5.926 eV. These results indicate that TGTPAT is very prone to react with the metallic surface using two ways of electron transfer (inhibitor to metal and *vice versa*) [55]. The dipole moment (μ) is a very important quantum chemical parameter that resulted from the non-uniformed distribution of charges on various atoms in the inhibitor compound. According to the literature, a good corrosion inhibitor has a high (μ) value tends to form strong dipole-dipole interactions with the metallic surface [56]. In our case, the studied compound is associated with the very highest values of dipole moment(μ) as follows: 6.332 (Debye). These results indicate that this molecule is very reactive and interacts strongly with the E24-surface during its contact with it. The electronegativity (χ) is an important factor that explains the stability and chemical reactivity of a molecule. A low value of (χ) suggests that inhibitor compound is highly potent to donate/transfer its electron to the metal surface [57]. The TGTPAT shows the (χ) values of 3.368 eV. The obtained electronegativity values show that this molecule is a good inhibitor [58]. Hardness (η) and softness (*S*) are another important quantum descriptor for estimating molecular stability and reactivity [58]. The low value of (η) is related with high reactivity; higher capacity of electron donor and therefore, high inhibition efficiency and the converse is true for (*S*) [59]. The calculated hardness and softness of title compound by DFT method is 2.963 eV and 0.337 eV, respectively.

Table 6. Molecular electronic structure parameters of title molecule employing TGTPAT computed at DFT-B3LYP/6-311++G(d,p) computations level in aqueous phase.

Descriptor	DFT B3LYP/6-311++G(d,p)
E_{HOMO} (eV)	–6.331
E_{LUMO} (eV)	–0.405
ΔE_{gap} (eV)	5.926
I (eV)	6.331
A (eV)	0.405
μ (Debye)	6.332
χ (eV)	3.368
η (eV)	2.963
S (eV^{-1})	0.337
ω (eV)	1.914
ε (eV^{-1})	0.522
ΔN_{110}	0.245
Δψ	0.177
E (Hartree)	–1601.6879

This trend suggested that this compound is reactive and have a high absorption capacity on the metal surface. Similarly, the electrophilicity index (ω) and nucleophilicity index values (ε) for the studied compound were also computed. Lower and higher values of (ω) and (ε), respectively suggest that the compound is a good nucleophile (donor) and electrophile (acceptor), consequently a good corrosion inhibitor [60]. As shown in Table 6, our compound is associated with a very low electrophilicity index and high nucleophilicity index values regardless of the method. This reflects the higher tendency to donor-acceptor electrons to the E24-surface of title molecule. The values (ΔN) represent the number of electron donation exchanged between inhibitor to the metal surface. When $\Delta N > 0$, and *vice versa* if $\Delta N < 3.6$, the inhibition efficiency increases by increasing electron-donating ability at the E24-surface [61]. In our present study, the values of the number of electrons transferred of 0.245 eV was less than 3.6 indicating the tendency of this compound to donate electrons to the E24-surface. These results are in agreement with Lukovits' study [61]. Now we turn to examine the metal/inhibitor interaction energy (Δψ) index, which is an important parameter in terms of investigation of the anti-corrosion capacity of our molecule [61]. Our results reveal a Δψ of 0.177 eV; there is indicating that TGTPAT is a good inhibitor. On the other hand, the total E (Hartree) specified by the DFT calculations turned out to be –1601.6879 a.u. Therefore, the computational study indicated that TGTPAT at the B3LYP

level was more stable because all the substituents are equatorial [62]. Through the above and based on the quantum chemical parameters obtained, it is clear that the title compound is a good inhibitor against the corrosion of carbon steel in a corrosive medium.

3.6.4. Mulliken charge distribution and Molecular Electrostatic Potential (MEP)

The Mulliken atomic charges are typically used in quantum chemical calculations to identify active centers in the molecule that interact with metals. It has been confirmed in a number of studies that the higher the negative atomic charges of the adsorbed center, the easier it is for the atom to donate its electron to the unoccupied orbital of the metal [63]. The Mulliken charges of the atoms of the title molecule are presented in Figure 13. As shown in this figure, the nitrogen (N) and oxygen (O) atoms, as well as C=C bonds have negative charges with high electron density. These atoms, therefore, behave like the nucleophilic centers when they interact with the unoccupied orbital of the E24-surface to form coordinate bond. Also, in Figure 13, The Molecular Electrostatic Potential (MEP) was studied, which provides important information about the low and high electron density parts present in the inhibitor compound. As can be seen from Figure 13, the MEP is expressed on the area of the selected inhibitors in different colors where the red-orange-yellow colors display the area of the regions with strong electron density and blue for the location with low electron density [64]. It can be seen in neutral form of the title molecule that most of the strong electron density (electron-rich regions) is concerning the O /N atoms and C=C bonds. These regions are believed to have the greatest ability to donate electrons on the unoccupied (d) orbitals of Fe-atoms and therefore have higher interactions onto the Fe surface [65].

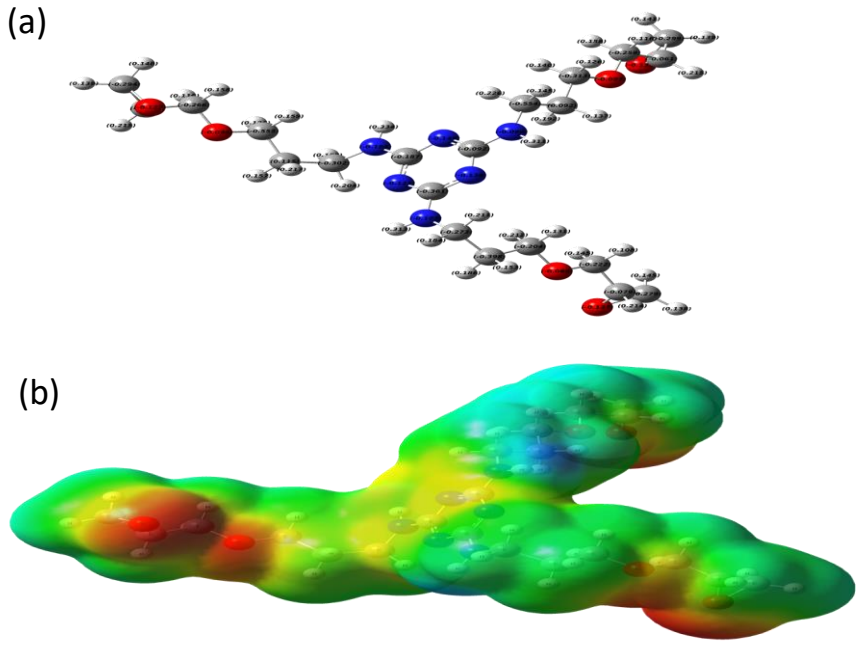

Figure 13. (a) Mulliken charges and (b) Molecular Electrostatic Potential of TGTPAT.

3.7. MD /MC modeling

The Monte Carlo (MC) and molecular dynamics (MD) simulations were used in our current study to clarify the behavior of the system (single inhibitor molecule in neutral form / E24-surface / corrosive species) and to better understand the inhibitory characteristics of the studied substance. The most stable (low energy) arrangement of the corrosion inhibitor chemical (adsorbate) on the E24-surface (substrate) may be reliably predicted using MC/MD simulations [66, 67]. The most stable low-energy adsorption sites are determined by running MC/MD simulations of the configurational space for the inhibitor compound onto the E24-surface with various molecule-surface bond lengths, as shown in Figure 14. These equilibrated snapshots reveal that the suggested corrosion inhibitor is adsorbed on the Fe surface in neutral form, with the O/N atoms and C=C bonds oriented planarly to the metal surface. These sites operate as reactive sites when the inhibitor interacts with the E24 surface [68]. Corrosion inhibitors prevent corrosion by adsorbing on the metal surface and receiving electrons from the metal surface as well as donating electrons through heteroatoms / C=C bonds [69]. Furthermore, the title molecule's (TGTPAT) structure appears to take the place of water (H_2O) molecules and H_3O^+/Cl^- ions in a corrosive media, providing a more stable site on the E24-surface. Figure 15 depicts the adsorption energy distribution for the E24/TGTPAT/500H_2O/6H_3O^+/6Cl^- interface generated by MC simulation.

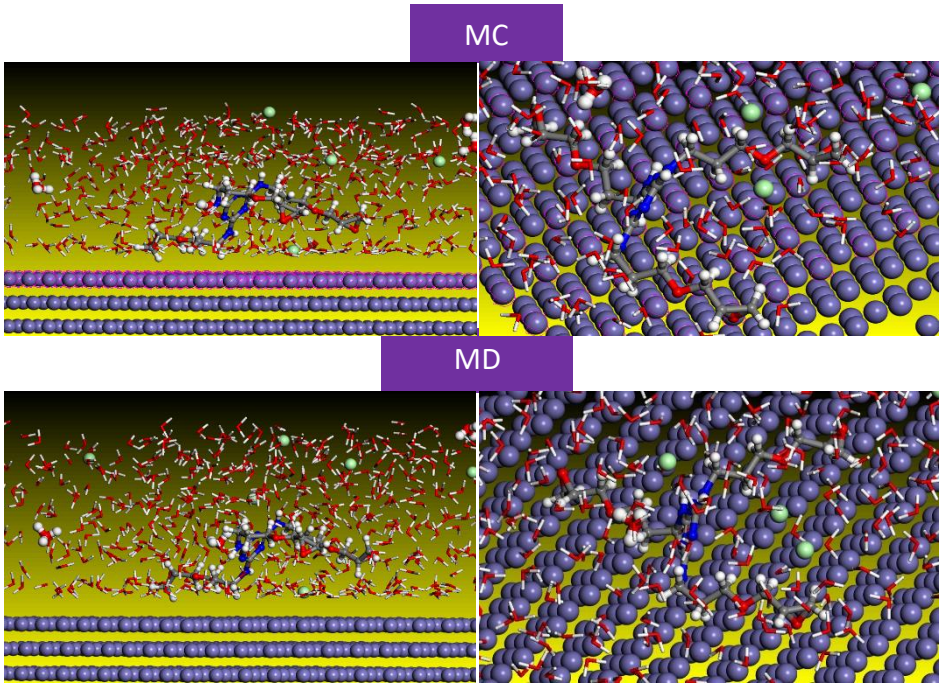

Figure 14. Snapshots of TGTPAT over E24-surface obtained from MD / MC simulations.

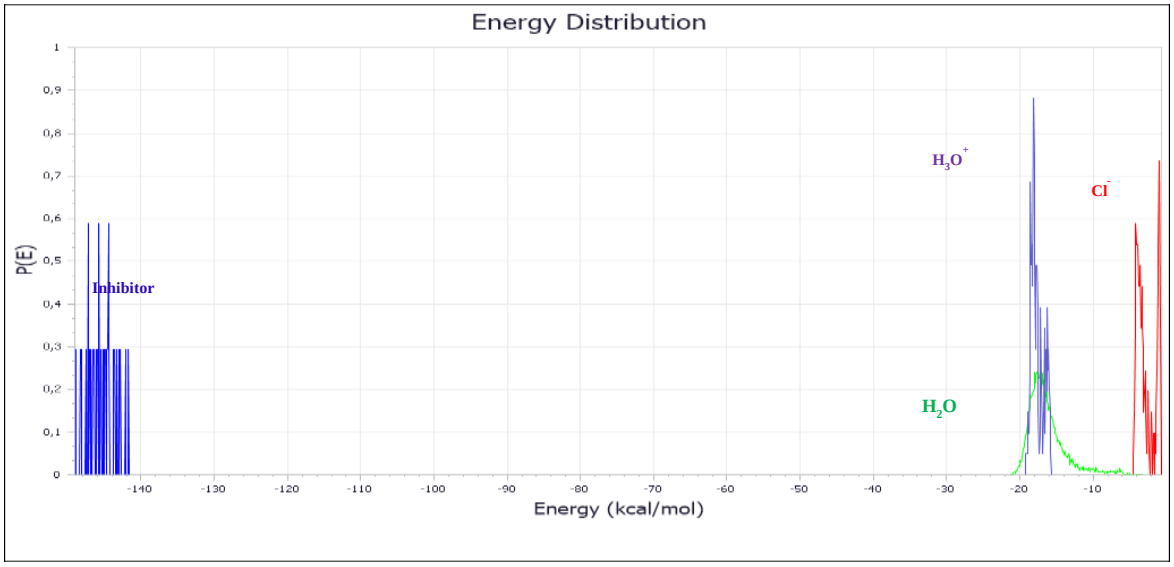

Figure 15. Adsorption energy distribution for the (E24/TGTPAT/500H_2O/6H_3O^+/6Cl^-) system obtained by the MC simulations.

A lower adsorption energy (E_{ads}) value suggests stronger and more spontaneous contacts between the inhibitor chemical and the metal surface [70]. As demonstrated in Figure 15, the adsorption energy of TGTPAT approaches –149 kcal/mol, indicating that TGTPAT has high absorption on the iron surface. The kinetics of inhibitor adsorption on metal surfaces may be monitored and studied using MD simulations. One way to make sure the components contain the least amount of energy is to keep track of any temperature changes that take place during the MD simulation run [45]. For equilibrium contact with a certain temperature requirement, the temperature distribution generated by the MD simulation should be limited to 5–15%. [71]. Based on the temperature graphs for the E24/ TGTPAT/500H2O/6H_3O^+/6Cl^- system calculated by MD at 293 K (Figure 16). Minor temperature changes during the MD simulation indicate that the run was successful, implying that all systems have reached their equilibrium states.

Table 7 shows the computed and stated energy characteristics of adsorbed TGTPAT in the aqueous phase. It is important to note that greater and lower adsorption energy (E_{ads}) values imply more stable/easier adsorption onto the E24 surface, as well as higher inhibitory effectiveness [72, 73]. According to Table 7, the E_{ads} of TGTPAT is close to –4614.93 kcal/mol in solution phases, showing that the title molecule (TGTPAT) interacts strongly with the iron-based layer and forms a protective adsorbed film.

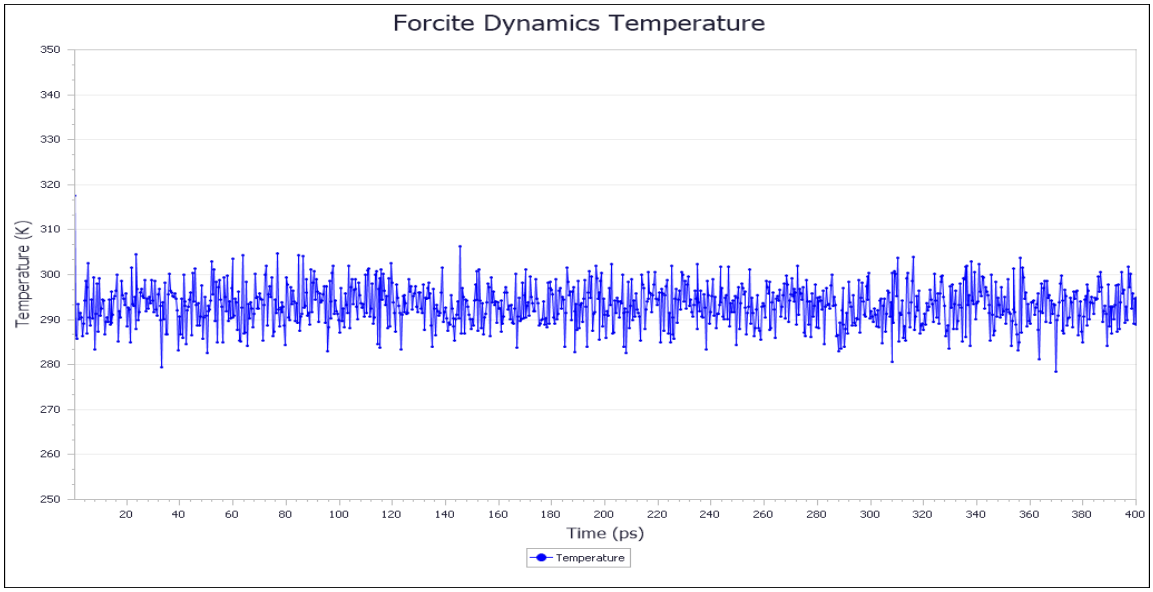

Figure 16. Temperature equilibrium curves for E24/TGTPAT/500H_2O/6H_3O^+/6Cl^- system by the MD simulations.

Table 7. MC simulations descriptors for the adsorption of TGTPAT in aqueous phases over the E24 surface (all values in kcal/mol).

System	E_{tot}	E_{ads}	E_{RA}	E_{def}	$dE_{ads}/dNi_{inhibitor}$	dE_{ads}/dNi_{H2O}	dE_{ads}/dNi_{H3O}^+	dE_{ads}/dNi_{Cl}^-
E24/ TGTPAT/ 500H_2O/6H_3O^+/6Cl^-	–2790.85	–4614.93	–3915.20	–699.72	–147.20	–2.87	–16.40	–0.87

The radial distribution function (RDF) method is also used to determine the type of bonds (physical, chemical, or both) formed between the TGTPAT structure and iron atoms. Chemisorption is often utilized when the bond length value is between 1–3.5 Å, whereas physisorption (Van der Waals and Coulomb interactions) is typically employed when the bond length value is larger than 3.5 Å [49]. Figure 17 shows the RDF of the TGTPAT by MD trajectory. All the initial peak values for TGTPAT in solution phases are less than 3.5 Å (chemisorption range) (Figure 17). These are the most essential interactions of the modelled

structures of the title molecule on the E24-surface, revealing that the title molecule does indeed impede the disintegration of the tested metal.

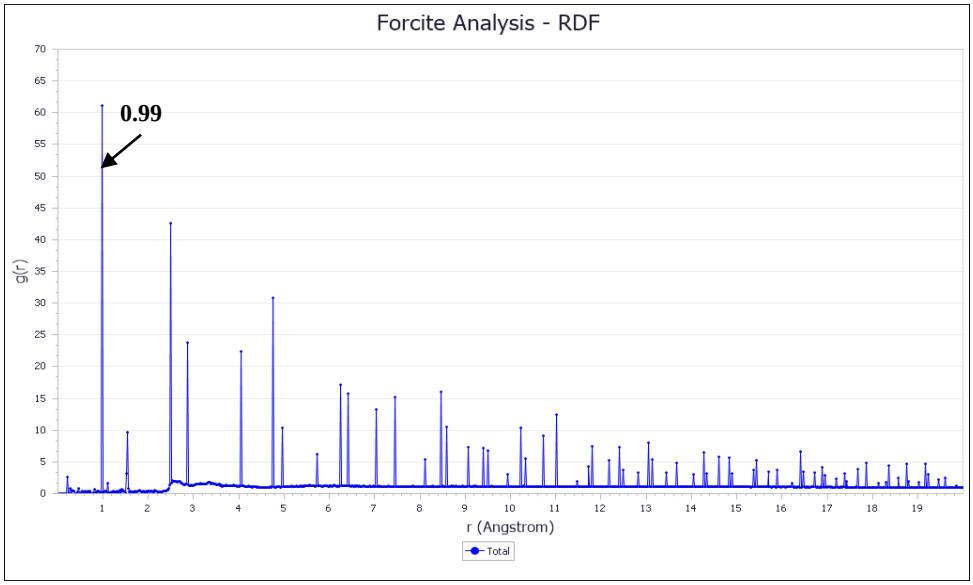

Figure 17. RDF of the TGTPAT on the E24-surface in corrosive medium.

Conclusion

We used stationary and transient electrochemical methods such as polarization curves and electrical impedance spectroscopy to test the inhibitory effect of an organic compound called triglycidyloxy tripropylamine triazine (TGTPAT). The main results of this study, which we have achieved, can be summarized as follows:

- TGTPAT showed good positive behavior in the protection against corrosion of E24 steel in 1 M HCl acid medium, with a maximum inhibitory efficiency of 92.11% at a concentration of 10^{-3} mol/l and a temperature of 293 K.
- Manipulation at different temperatures (293 K to 323 K) shows that the TGTPAT inhibitory effectiveness decreases with increasing temperature. The polarization study revealed that the inhibitor is of mixed type.
- Analysis of the derived standard free energy reveals that the adsorption on the steel surface is chemisorption and follows the Langmuir adsorption isotherm.

The values and results obtained from the two techniques, namely polarization curves and electrochemical impedance spectroscopy as a function of the concentration of the inhibitor compound, show good agreement with the electronic and atomic analyses of the inhibitor based, respectively, on DFT calculations and molecular dynamics simulations, which substantiate its ability to act as a powerful anti-corrosion agent for E24 steel in 1 M HCl medium.

References

1. C. Lee, W. Yang and R.G. Parr, Development of the Colle-Salvetti correlation-energy formula into a functional of the electron density, *Phys. Rev*., 1988, **37**, no. 2, 785. doi: 10.1103/PhysRevB.37.785
2. K. Azgaou, M. Damej, S. El Hajjaji, N.K. Sebbar, H. Elmsellem, B. El Ibrahimi and M. Benmessaoud, Synthesis and characterization of N-(2-aminophenyl)-2-(5-methyl-1H-pyrazol-3-yl) acetamide (AMPA) and its use as a corrosion inhibitor for C38 steel in 1 M HCl. Experimental and theoretical study, *J. Mol. Struct*., 2022, **1266**, 133451. doi: 10.1016/j.molstruc.2022.133451
3. N. Chaubey, Savita, V.K. Singh and M.A. Quraishi, Corrosion inhibition performance of different bark extracts on aluminium in alkaline solution, *J. Assoc. Arab Univ. Basic Appl. Sci*., 2017, **22**, no. 1, 38–44. doi: 10.1016/j.jaubas.2015.12.003
4. J. Tomasi, B. Mennucci and R. Cammi, Quantum Mechanical Continuum Solvation Model, *Chem. Rev*., 2005, **105**, no. 8, 2999–3094. doi: 10.1021/cr9904009

[5] Z. Lakbaibi, M. Damej, A. Molhi, M. Benmessaoud, S. Tighadouini, A. Jaafar, T. Benabbouha, A. Ansari, A. Driouich and M. Tabyaoui, Evaluation of inhibitive corrosion potential of symmetrical hydrazine derivatives containing nitrophenyl moiety in 1 M HCl for C38 steel: experimental and theoretical studies, *Heliyon*, 2022, **8**, no. 3, e09087. doi: 10.1016/j.heliyon.2022.e09087

6. A. Chraka, I. Raissouni, N.B. Seddik, S. Khayar, S. El Amrani, M. El Hadri, F. Chaouket and D. Bouchta, Croweacin and Ammi visnaga (L.) Lam Essential Oil derivatives as green corrosion inhibitors for brass in 3% NaCl medium: Quantum Mechanics investigation and Molecular Dynamics Simulation Approaches, *Mediterr. J. Chem*., 2020, **10**, no. 4, 378. doi: 10.13171/mjc10402004281338ac
7. A. Chraka, I. Raissouni, N. Benseddik, S. Khayar, A.I. Mansour, H. Belcadi, F. Chaouket and D. Bouchta, Aging time effect of *Ammi visnaga* (L.) lam essential oil on the chemical composition and corrosion inhibition of brass in 3% NaCl medium. Experimental and theoretical studies, *Mater. Today Proc*., 2020, **22**, 83–88. doi: 10.1016/j.matpr.2019.08.086
8. A. Ouaket, A. Chraka, I. Raissouni, M.A. El Amrani, M. Berrada and N. Knouzi, Synthesis, spectroscopic ($^{13}C/^{1}H$-NMR, FT-IR) investigations, quantum chemical modelling (FMO, MEP, NBO analysis), and antioxidant activity of the bis-benzimidazole molecule, *J. Mol. Struct*., 2022, **1259**, 132729. doi: 10.1016/j.molstruc.2022.132729
9. N. Metropolis, S. Ulam, The Monte Carlo Method, *J. Am. Stat. Assoc*., 1949, **44**, no. 247, 335–341. doi: 10.1080/01621459.1949.10483310
10. M. Abouchane, R. Hsissou, A. Molhi, M. Damej, K. Tassaoui, A. Berisha, A. Chraka and M. Benmessaoud, Exploratory Experiments Supported by Modeling Approaches for TGEEA New Epoxy Resin as a Contemporary Anti-corrosion Material for C38 Steel in

1.0 M HCl, *J. Fail. Anal. Prev*., 2023, **23**, no. 4, 1765–1781. doi: 10.1007/s11668-023-01705-9

11. M. Errili, A. Al Maofari, K. Tassaoui, M. Damej, Z. Lakbaibi, A. Et-Tahir, S. El Hajjaji and M. Benmessaoud, Electrochemical and theoretical (DFT, MC, MD) evaluation of a new compound based on mercaptobenzimidazole against corrosion of Cu-30Ni in a 3% NaCl solution, *Int. J. Corros. Scale Inhib*., 2023, **11**, 458–476. doi: 10.17675/2305-6894-2023-12-2-5
12. K. Tassaoui, A. Al-Shami, M. Damej, A. Molhi, O. Mounkachi and M. Benmessaoud, Contribution to the corrosion inhibitors of copper-nickel (Cu-30Ni) in 3% NaCl solution by two new molecules of triazole: Electrochemical and theoretical studies, *J. Mol. Struct*., 2023, **1291**, 135836. doi: 10.1016/j.molstruc.2023.135836
13. H. Sun, Ren and J.R. Fried, The COMPASS force field: parameterization and validation for phosphazenes, *Comput. Theor. Polym. Sci*., 1998, **8**, no. 1, 229–246. doi: 10.1016/S1089-3156(98)00042-7
14. H. Bourzi, R. Oukhrib, B. El Ibrahimi, H. Abou Oualid, Y. Abdellaoui, B. Balkard, S. El Issami, M. Hilali, L. Bazzi and C. Len, *Sustainability*, 2020, **12**, no. 8, 3304. doi: 10.3390/su12083304
15. A. Chraka, N.B. Seddik, I. Raissouni, J. Kassout, M. Choukairi, M. Ezzaki, O. Zaraali, H. Belcadi, F. Janoub and A.I. Mansour, Electrochemical explorations, SEM/EDX analysis, and quantum mechanics/molecular simulations studies of sustainable corrosion inhibitors on the Cu-Zn alloy in 3% NaCl solution, *J. Mol. Liq*., 2023, **387**, 122715. doi: 10.1016/j.molliq.2023.122715
16. L. Amini, S. Zouitina, A. Chraka, A. Moubarik, K. El Harfi and M. Mbarki, Theoretical Evaluation of Ibuprofen and Paracetamol by Fukui and Parr Functions Descriptors: DFT Study, in *2020 IEEE 6th International Conference on Optimization and Applications (ICOA)*, 2020, 1–5. doi: 10.1109/ICOA49421.2020.9094523
17. R. Hsissou, K. Dahmani, A. El Magri, A. Hmada, Z. Safi, N. Dkhireche, M. Galai, N. Wazzan and A. Berisha, A Combined Experimental and Computational (DFT, RDF, MC and MD) Investigation of Epoxy Resin as a Potential Corrosion Inhibitor for Mild Steel in a 0.5 M H_2SO_4 Environment, *Polymers*, 2023, **15**, no. 8, 1967. doi: 10.3390/polym15081967
18. H. Bouayadi, M. Damej, A. Molhi, Z. Lakbaibi, M. Benmessaoud and M. Cherkaoui, Electrochemical and theoretical evaluation of thiocarbohydrazide as a brass (60/40) corrosion inhibitor in 3% NaCl solution and effect of temperature on this process, *Int. J. Corros. Scale Inhib*., 2022, **11**, no. 3, 1335–1354. doi: 10.17675/2305-6894-2022-11-3-25
19. H. Belcadi, A. Chraka, S. El Amrani, I. Raissouni, A. Moukhles, S. Zantar, L. Toukour and A.I. Mansour, Investigation and Valorization of the Moroccan *Salvia Officinalis* L. Essential Oil: Phytochemistry, Potential in Corrosion Inhibition, Antibacterial Activity, and Theoretical Modeling, *J. Bio Tribo Corros*., 2023, **9**, no. 3, 50. doi: 10.1007/s40735-023-00769-2

20. M. Belhadi, M. Oubahou, I. Hammoudan, A. Chraka, M. Chafi and S. Tighadouini, A comprehensive assessment of carbon steel corrosion inhibition by 1,10-phenanthroline in the acidic environment: insights from experimental and computational studies, *Environ. Sci. Pollut. Res*., 2024, **31**, 62038–62055. doi: 10.1007/s11356-023-27582-1
21. A. Chraka, I. Raissouni, N.B. Seddik, S. Khayar, A.I. Mansour, S. Tazi, F. Chaouket and D. Bouchta, Identification of Potential Green Inhibitors Extracted from *Thymbra capitata* (L.) Cav. for the Corrosion of Brass in 3% NaCl Solution: Experimental, SEM–EDX Analysis, DFT Computation and Monte Carlo Simulation Studies, *J. Bio Tribo Corros*., 2020, **6**, no. 3, 80. doi: 10.1007/s40735-020-00377-4
22. K. Tassaoui, M. Damej, A. Molhi, A. Berisha, M. Errili, S. Ksama, V. Mehmeti, S. El Hajjaji and M. Benmessaoud, Contribution to the corrosion inhibition of Cu–30Ni copper–nickel alloy by 3-amino-1,2,4-triazole-5-thiol (ATT) in 3% NaCl solution. Experimental and theoretical study (DFT, MC and MD), *Int. J. Corros. Scale Inhib*., 2022, **11**, no. 1, 221–244. doi: 10.17675/2305-6894-2022-11-1-12
23. Z. Akounach, A. Al Maofari, M. Damej, S. El Hajjaji, A. Berisha, V. Mehmeti, N. Labjar, M. Bamaarouf and M. Benmessaoud, Contribution to the corrosion inhibition of aluminum in 1 M HCl by Pimpinella Anisum extract. Experimental and theoretical studies (DFT, MC, and MD), *Int. J. Corros. Scale Inhib*., 2022, **11**, no. 1, 402–424. doi: 10.17675/2305-6894-2022-11-1-24
24. M. Damej, A. Molhi, H. Lgaz, R. Hsissou, J. Aslam, M. Benmessaoud, N. Rezki, H. Lee and D. Lee, Performance and interaction mechanism of a new highly efficient benzimidazole-based epoxy resin for corrosion inhibition of carbon steel in HCl: A study based on experimental and first-principles DFTB simulations, *J. Mol. Struct*., 2023, **1273**, 134232. doi: 10.1016/j.molstruc.2022.134232
25. Noudem, D. Fouejio, C. Mveme, S. Zekeng, F.T. Nya and G. Ejuh, Hartree-Fock and DFT studies of the optoelectronic, thermodynamic, structural and nonlinear optical properties of photochromic polymers containing styrylquinoline fragments, *Mater. Chem. Phys*., 2022, **281**, 125883. doi: 10.1016/j.matchemphys.2022.125883
26. M.J. Dewar and W. Thiel, Ground states of molecules. 38. The MNDO method. Approximations and parameters, *J. Am. Chem. Soc*., 1977, **99**, no. 15, 4899–4907. doi: 10.1021/ja00457a004
27. B. Gómez, N.V. Likhanova, M.A. Domínguez-Aguilar, R. Martínez-Palou, A. Vela and J.L. Gazquez, Quantum Chemical Study of the Inhibitive Properties of 2-Pyridyl-Azoles, *J. Phys. Chem. B*, 2006, **110**, no. 18, 8928-8934. doi: 10.1021/jp057143y
28. R. Hasanov, M. Sadıkoğlu and S. Bilgiç, Electrochemical and quantum chemical studies of some Schiff bases on the corrosion of steel in H_2SO_4 solution, *Appl. Surf. Sci*., 2007, **253**, no. 8, 3913–3921. doi: 10.1016/j.apsusc.2006.08.025
29. C. Verma, J. Haque, E.E. Ebenso and M. Quraishi, Melamine derivatives as effective corrosion inhibitors for mild steel in acidic solution: Chemical, electrochemical, surface and DFT studies, *Results Phys*., 2018, **9**, 100–112. doi: 10.1016/j.rinp.2018.02.018

30. K. Tassaoui, A. Al-Shami, M. Damej, A. Molhi, O. Mounkachi and M. Benmessaoud, Contribution to the corrosion inhibitors of copper-nickel (Cu-30Ni) in 3% NaCl solution by two new molecules of triazole: Electrochemical and theoretical studies, *J. Mol. Struct*., 2023, **1291**, 135836. doi: 10.1016/j.molstruc.2023.135836
31. N. Obi-Egbedi, I. Obot and M.I. El-Khaiary, Quantum chemical investigation and statistical analysis of the relationship between corrosion inhibition efficiency and molecular structure of xanthene and its derivatives on mild steel in sulphuric acid, *J. Mol. Struct*., 2011, **1002**, no. 1, 86–96. doi: 10.1016/j.molstruc.2011.07.003
32. S. Kaya, B. Tüzün, C. Kaya and I.B. Obot, Determination of corrosion inhibition effects of amino acids: Quantum chemical and molecular dynamic simulation study, *J. Taiwan Inst. Chem. Eng*., 2016, **58**, 528–535. doi: 10.1016/j.jtice.2015.06.009
33. M. Ouakki, M. Galai, M. Rbaa, A.S. Abousalem, B. Lakhrissi, E Rifi and M. Cherkaoui, Investigation of imidazole derivatives as corrosion inhibitors for mild steel in sulfuric acidic environment: experimental and theoretical studies, *Ionics*, 2020, **26**, no. 10, 5251–5272. doi: 10.1007/s11581-020-03643-0
34. I. Lukovits, E. Kalman and F. Zucchi, Corrosion Inhibitors—Correlation between Electronic Structure and Efficiency, *Corrosion*, 2001, **57**, no. 1, 3–8. doi: 10.5006/1.3290328
35. N. Abdelshafi, M.A. Ibrahim, A.-S. Badran and S.A. Halim, Experimental and theoretical evaluation of a newly synthesized quinoline derivative as corrosion inhibitor for iron in 1.0 M hydrochloric acid solution, *J. Mol. Struct*., 2022, **1250**, 131750. doi: 10.1016/j.molstruc.2021.131750
36. A. Bouoidina, F. El-Hajjaji, K. Emran, M.E. Belghiti, A. Elmelouky, M. Taleb, A. Abdellaoui, B. Hammouti and I.B. Obot, Towards Understanding the Anticorrosive Mechanism of Novel Surfactant Based on *Mentha pulegium* Oil as Eco-friendly Bio-source of Mild Steel in Acid Medium: a Combined DFT and Molecular Dynamics Investigation, *Chem. Res. Chin. Univ*., 2019, **35**, no. 1, 85–100. doi: 10.1007/s40242-019-8205-7
37. I. Obot, Z. Gasem and S. Umoren, Pyrazine derivatives as green oil field corrosion inhibitors for steel, *J. Mol. Liq*., 2019, **277**, 749–761. doi: 10.1016/j.molliq.2018.12.108
38. J. Saranya, F. Benhiba, N. Anusuya, R. Subbiah, A. Zarrouk and S. Chitra, Experimental and computational approaches on the pyran derivatives for acid corrosion, *Colloids Surf. Physicochem. Eng. Asp*., 2020, **603**, 125231. doi: 10.1016/j.colsurfa.2020.125231
39. Z. Sanaei, M. Ramezanzadeh, G. Bahlakeh and B. Ramezanzadeh, Use of *Rosa canina* fruit extract as a green corrosion inhibitor for mild steel in 1 M HCl solution: A complementary experimental, molecular dynamics and quantum mechanics investigation, *J. Ind. Eng. Chem*., 2019, **69**, 18–31. doi: 10.1016/j.jiec.2018.09.013
40. M. Damej, M. Benmessaoud, S. Zehra, S. Kaya, H. Lgaz, A. Molhi, N. Labjar, S. El Hajjaji, A.A. Alrashdi and H.-S. Lee, Experimental and theoretical explorations of S-alkylated mercaptobenzimidazole derivatives for use as corrosion inhibitors for carbon steel in HCl, *J. Mol. Liq*., 2021, **331**, 115708. doi: 10.1016/j.molliq.2021.115708

41. M. Damej, M. Abouchane, M. Doubi, H. Erramli, M. Benmessaoud and N. Hajjaji, Electrodeposition and Characterization of Poly 3-Amino-1,2,4-Triazole-5-Thiol Films on Brass Electrode in 0.1 M Methanol, *Coatings*, 2022, **12**, no. 11, Art. no. 11. doi: 10.3390/coatings12111784
42. I. Eliboev, E. Berdimurodov, K. Yakhshinorov, J. Abdisattarov, O. Dagdag, A. Berisha, W.W. Nik, A. Kholikov and K. Akbarov, Supramolecular corrosion protection: Eco-friendly synthesis and efficacy of a β-cyclodextrin/o-phenylenediamine complex, *J. Taiwan Inst. Chem. Eng*., 2023, **147**, 104944. doi: 10.1016/j.jtice.2023.104944
43. M. Damej, R. Hsissou, A. Berisha, K. Azgaou, M. Sadiku, M. Benmessaoud and N. Labjar, New epoxy resin as a corrosion inhibitor for the protection of carbon steel C38 in 1 M HCl. Experimental and theoretical studies (DFT, MC, and MD), *J. Mol. Struct*., 2022, **1254**, 132425. doi: 10.1016/j.molstruc.2022.132425
44. N.B. Iroha, V.C. Anadebe, N.J. Maduelosi, L.A. Nnanna, L.C. Isaiah, O. Dagdag, A. Berisha and E.E. Ebenso, Linagliptin drug molecule as corrosion inhibitor for mild steel in 1 M HCl solution: Electrochemical, SEM/XPS, DFT and MC/MD simulation approach, *Colloids Surf. Physicochem. Eng. Asp*., 2023, **660**, 130885. doi: 10.1016/j.colsurfa.2022.130885
45. W. Daoudi, A. El Aatiaoui, O. Dagdag, K. Zaidi, R. Haldhar, S.-C. Kim, A. Oussaid, A. Aouinti, A. Berisha and F. Benhiba, Anti-Corrosion Coating Formation by a Biopolymeric Extract of *Artemisia herba-alba Plant*: Experimental and Theoretical Investigations, *Coatings*, 2023, **13**, no. 3, Art. no. 3. doi: 10.3390/coatings13030611
46. M. Belghiti, S. Echihi, A. Dafali, Y. Karzazi, M. Bakasse, H. Elalaoui-Elabdallaoui, L. Olasunkanmi, E. Ebenso and M. Tabyaoui, Computational simulation and statistical analysis on the relationship between corrosion inhibition efficiency and molecular structure of some hydrazine derivatives in phosphoric acid on mild steel surface, *Appl. Surf. Sci*., 2019, **491**, 707–722. doi: 10.1016/j.apsusc.2019.04.125
47. M. Rbaa, F. Benhiba, M. Galai, Ashraf S. Abousalem, M. Ouakki, Chin Hung Lai, B. Lakhrissi, C. Jama, I. Warad, M. Ebn Touhami and A. Zarrouk, Synthesis and characterization of novel Cu (II) and Zn (II) complexes of 5-{(2-Hydroxyethyl) sulfanyl] methyl}-8-hydroxyquinoline as effective acid corrosion inhibitor by experimental and computational testings, *Chem. Phys. Lett*., 2020, **754**, 137771. doi: 10.1016/j.cplett.2020.137771
48. A. Jmiai, B. El Ibrahimi, A. Tara, S. El Issami, O. Jbara and L. Bazzi, Alginate biopolymer as green corrosion inhibitor for copper in 1 M hydrochloric acid: Experimental and theoretical approaches, *J. Mol. Struct*., 2018, **1157**, 408–417. doi: 10.1016/j.molstruc.2017.12.060
49. V. Mehmeti and F.I. Podvorica, Experimental and Theoretical Studies on Corrosion Inhibition of Niobium and Tantalum Surfaces by Carboxylated Graphene Oxide, *Materials*, 2018, **11**, no. 6, Art. no. 6. doi: 10.3390/ma11060893

50. A. Dehghani, G. Bahlakeh, B. Ramezanzadeh and M. Ramezanzadeh, A combined experimental and theoretical study of green corrosion inhibition of mild steel in HCl solution by aqueous *Citrullus lanatus* fruit (CLF) extract, *J. Mol. Liq.*, 2019, **279**, 603–624. doi: 10.1016/j.molliq.2019.02.010
51. R.A.H. Al-Uqaily and S.A. Al-Bayaty, Study A Corrosion Inhibitor Of 1-Isoquinolinyl Phenyl Ketone for Mild Steel In Acidic Medium As HCl Acid, *J. Phys.: Conf. Ser*., 2019, **1294**, no. 5, 052014. doi: 10.1088/1742-6596/1294/5/052014
52. Y. Feng, S. Chen, W. Guo, Y. Zhang and G. Liu, Inhibition of iron corrosion by 5,10,15,20-tetraphenylporphyrin and 5,10,15,20-tetra-(4-chlorophenyl)porphyrin adlayers in 0.5M H_2SO_4 solutions, *J. Electroanal. Chem*., 2007, **602**, no. 1, 115–122. doi: 10.1016/j.jelechem.2006.12.016
53. I.B. Obot, D.D. Macdonald and Z.M. Gasem, Density functional theory (DFT) as a powerful tool for designing new organic corrosion inhibitors. Part 1: An overview, *Corros. Sci*., 2015, **99**, 1–30. doi: 10.1016/j.corsci.2015.01.037
54. K. Abderrahim, I. Selatnia, A. Sid and Mosset, 1,2-bis(4-chlorobenzylidene) Azine as new and effective corrosion inhibitor for copper in 0.1 N HCl: A combined experimental and theoretical approach, *Chem. Phys. Lett*., 2018, **707**, 117–128. doi: 10.1016/j.cplett.2018.07.046
55. E. Rodriguez-Clemente, J.G. Gonzalez-Rodriguez and M.G. Valladares-Cisneros, *Allium sativum* as Corrosion Inhibitor for Carbon Steel in Sulfuric Acid, *Int. J. Electrochem. Sci*., 2014, **9**, no. 11, 5924–5936. doi: 10.1016/S1452-3981(23)10859-5
56. I.B. Obot, N.O. Obi-Egbedi and S.A. Umoren, Adsorption Characteristics and Corrosion Inhibitive Properties of Clotrimazole for Aluminium Corrosion in Hydrochloric Acid, *Int. J. Electrochem. Sci*., 2009, **4**, no. 6, 863–877. doi: 10.1016/S1452-3981(23)15190-X
57. C.A. Loto, R.T. Loto and O.J. Oshogbunu, Corrosion inhibition effect of Allium sativum extracts on mild steel in HCl and H_2SO_4, *J. Chem. Pharm. Res*., 2016, **8**, no. 2, 216–230.
58. R. Hsissou, F. Benhiba, S. Abbout, O. Dagdag, S. Benkhaya, A. Berisha, H. Erramli amd A. Elharfi, Trifunctional epoxy polymer as corrosion inhibition material for carbon steel in 1.0 M HCl: MD simulations, DFT and complexation computations, *Inorg. Chem. Commun*., 2020, **115**, 107858. doi: 10.1016/j.inoche.2020.107858
59. W. Huang, L. Hu, C. Liu, J. Pan, Y. Tian and K. Cao, Corrosion Inhibition of Carbon Steel by Lepidine in HCl Solution, *Int. J. Electrochem. Sci*., 2018, **13**, no. 11, 11273–11285. doi: 10.20964/2018.11.90
60. R. Hasanov, M. Sadıkoğlu and S. Bilgiç, Electrochemical and quantum chemical studies of some Schiff bases on the corrosion of steel in H_2SO_4 solution, *Appl. Surf. Sci*., **253**, no. 8, 3913–3921. doi: 10.1016/j.apsusc.2006.08.025
61. C. Verma, J. Haque, E.E. Ebenso and M.A. Quraishi, Melamine derivatives as effective corrosion inhibitors for mild steel in acidic solution: Chemical, electrochemical, surface and DFT studies, *Results Phys*., 2018, **9**, 100–112. doi: 10.1016/j.rinp.2018.02.018

62. N.O. Obi-Egbedi, I.B. Obot and M.I. El-Khaiary, Quantum chemical investigation and statistical analysis of the relationship between corrosion inhibition efficiency and molecular structure of xanthene and its derivatives on mild steel in sulphuric acid, *J. Mol. Struct*., 2011, **1002**, no. 1, 86–96. doi: 10.1016/j.molstruc.2011.07.003
63. S. Kaya, B. Tüzün, C. Kaya and I.B. Obot, Determination of corrosion inhibition effects of amino acids: Quantum chemical and molecular dynamic simulation study, *J. Taiwan Inst. Chem. Eng*., 2016, **58**, 528–535. doi: 10.1016/j.jtice.2015.06.009
64. N.S. Abdelshafi, M.A. Ibrahim, A.-S. Badran and S.A. Halim, Experimental and theoretical evaluation of a newly synthesized quinoline derivative as corrosion inhibitor for iron in 1.0 M hydrochloric acid solution, *J. Mol. Struct*., 2022, **1250**, 131750. doi: doi.org/10.1016/j.molstruc.2021.131750
65. M.O. Sidine, H. Lahbib, M. Ba, A.M.V. Salihi, M. Benmessaoud, Y.B. Amor and B.O. Elemine, Corrosion inhibition of XC48 steel by Grewia bicolor jus leaves extract in 1M HCL acid medium: electrochemical and gravimetric study, *Egyptian J. Chem*., 2024, **67**, no. 4, 181–191. doi: 10.21608/ejchem.2023.229759.8472
66. I.B. Obot, Z.M. Gasem and S.A. Umoren, Understanding the Mechanism of 2-mercaptobenzimidazole Adsorption on Fe (110), Cu (111) and Al (111) Surfaces: DFT and Molecular Dynamics Simulations Approaches, *Int. J. Electrochem. Sci*., 2014, **9**, no. 5, 2367–2378. doi: 10.1016/S1452-3981(23)07933-6
67. I.B. Obot, S.A. Umoren, Z.M. Gasem, R. Suleiman and B.E. Ali, Theoretical prediction and electrochemical evaluation of vinylimidazole and allylimidazole as corrosion inhibitors for mild steel in 1M HCl, *J. Ind. Eng. Chem*., 2015, **21**, 1328–1339. doi: 10.1016/j.jiec.2014.05.049
68. B.E. Ibrahimi, L. Bazzi and S.E. Issami, The role of pH in corrosion inhibition of tin using the proline amino acid: theoretical and experimental investigations, *RSC Adv*., 2020, **10**, no. 50, 29696–29704. doi: 10.1039/D0RA04333H
69. I. Ahamad, R. Prasad and M.A. Quraishi, Thermodynamic, electrochemical and quantum chemical investigation of some Schiff bases as corrosion inhibitors for mild steel in hydrochloric acid solutions, *Corros. Sci*., 2010, **52**, no. 3, 933–942. doi: 10.1016/j.corsci.2009.11.016
70. O.K. Abiola and N.C. Oforka, Adsorption of (4-amino-2-methyl-5-pyrimidinyl methylthio) acetic acid on mild steel from hydrochloric acid solution (HCl)—Part 1, *Mater. Chem. Phys*., 2004, **83**, no. 2, 315–322. doi: 10.1016/j.matchemphys.2003.10.001
71. H. Bourzi, R. Oukhrib, B. El Ibrahimi, H.A. Oualid, Y. Abdellaoui, B. Balkard, M. Hilali and S. El Issami, Understanding of anti-corrosive behavior of some tetrazole derivatives in acidic medium: Adsorption on Cu (111) surface using quantum chemical calculations and Monte Carlo simulations, *Surf. Sci*., 2020, **702**, 121692. doi: 10.1016/j.susc.2020.121692
72. R. Oukhrib, B. El Ibrahimi, H.A. Oualid, Y. Abdellaoui, S. El Issami, L. Bazzi, M. Hilali and H. Bourzi, In silico investigations of alginate biopolymer on the Fe (110), Cu (111), Al (111) and Sn (001) surfaces in acidic media: Quantum chemical and molecular

mechanic calculations, *J. Mol. Liq.*, 2020, **312**, 113479. doi: 10.1016/j.molliq.2020.113479

73. V. Mehmeti and F.I. Podvorica, Experimental and Theoretical Studies on Corrosion Inhibition of Niobium and Tantalum Surfaces by Carboxylated Graphene Oxide, *Materials*, 2018, **11**, no. 6, Art. no. 6.; doi: 10.3390/ma11060893

♦ ♦ ♦